



Supplementary Information for Soft cells and the geometry of seashells

Gábor Domokos, Alain Goriely, Ákos G. Horváth and Krisztina Regős

Gábor Domokos
Email: domoks@iit.bme.hu

This PDF file includes:

Supplementary text
Figures S1 to S27

Other supplementary materials for this manuscript include the following:

Supporting Movie SM1, “The edge bending algorithm”.

6 **Contents**

7	1 Proof of the main theorem	2
8	A Definition of polyhedral tilings and soft nodes	2
9	B Definition of the edge bending algorithm	3
10	C The general combinatorial condition for node softening: Lemma 1 and its proof	4
11	D An easy-to-check sufficient condition for node softening: proof of Theorem 1	6
12	2 Analytical examples of soft monohedral tilings	7
13	A The soft tetrahedral space-filler	9
14	B Prismatic monohedric tilings with rotational symmetries	11
15	B.1 Triangular prism	11
16	B.2 Squared prism	12
17	B.3 Hexagonal prism	12
18	3 Additional geometric concepts	12
19	A The geometry of z-cells	12
20	B The softness of rotational ellipsoids	13
21	4 Illustration of soft monohedral tilings	14
22	A Detailed illustration of the 7 soft cells shown in Figure 4, panels (d1-d4,f1-f3) of the main text	14
23	B Soft cells appearing in art	15
24	B.1 Soft 3D cells in architectural design	15
25	B.2 Soft 2D cells in fine art	15
26	5 Space filling properties of sea shell chambers	16
27	A Seilacher's models and the chamber of the Nautilus	16
28	A.1 The balloon model	17
29	A.2 The paper model	19
30	B Ammonite shells	20

31 **1. Proof of the main theorem**

32 For easier reference, we repeat the Theorem stated in the body of the main manuscript.

33 **Theorem 1** Let M be a balanced, normal convex tiling and let $\mathcal{V}(M)$ denote the set of the duals of vertex polyhedra in M . If
34 in the edge graph of every polyhedron $P \in \mathcal{V}(M)$ there exists a Hamiltonian circuit, then there exists a soft polyhedral tiling M'
35 which is combinatorially equivalent to M .

36 Our goal is to prove Theorem 1. We will also prove that if an edge graph is simple, the condition of the existence of a
37 Hamiltonian circuit can be weakened for the existence of a Hamiltonian path. We also remark that we will rely on the concepts
38 and definitions given in the Materials and Methods section of the main manuscript. For easier reference we repeat those
39 concepts below.

40 **A. Definition of polyhedral tilings and soft nodes.** Polyhedral tilings (1) are a remarkable class of space-filling tessellations
41 with the special property that each cell is a polyhedron having flat faces and straight edges. The significance of this class of
42 tilings is perhaps best illustrated by the fact that all convex tilings are polyhedral (2). Below we introduce one of the central
43 concepts of the paper, which is a generalization of polyhedral tilings to *polyhedral tilings*, admitting curved edges and faces,

44 Let M be a normal, balanced tiling (1) of \mathbb{R}^d ($d = 2, 3$) and let $P \in \mathbb{R}^d$ ($d = 2, 3$) be a point. More precisely, in this paper
45 we assume that the cells are topological closed d -balls of \mathbb{R}^d ($d = 2, 3$) with non-empty pairwise disjoint interiors with the
46 property that the intersection of any two of them is also a closed topological ball of less dimension. The cells of the tiling are
47 uniformly bounded, and the limit process which are needed to our mean-field theory are independent from the position of the
48 center of the sequence of concentric Euclidean spheres. In space, these assumptions give a large class of tilings which we would
49 like to exclude from our investigation. Hence we define a class of tilings which is a modest generalization of polyhedral tilings.
50 We define first the type of points with respect to the given tiling.

51 **Definition 1** Let $C(P)$ denote the number of cells containing P . Let S_P^D be a D -dimensional topological ball containing P in
52 its interior. Let $D(P) = D_0$ if D_0 is the largest integer for which $\exists S_P^{D_0}$ such that $\forall P' \in S_P^{D_0}$ we have $C(P') = C(P)$. We call
53 the pair $(C(P), D(P))$ the type of the point P with respect to the tiling M .

54 These three point types are illustrated in Figure S1 for a rectangular grid.

55 **Definition 2** In $d = 2$ dimensions, we call the connected components of type $(x, 2)$ points open cells. The boundary of a cell is
56 composed of the disjoint union of relative open edges consisting of type $(y, 1)$ points and of type $(n, 0)$ points which are the
57 nodes of the cell.

58 Note that the open edges of the tiling are the connected components of the set of type $(y, 1)$ points, separated by the nodes.

59 **Definition 3** In $d = 3$ dimensions we call the connected components of type $(x, 3)$ points open cells. The boundary of a cell is
60 the union of relative open faces formed by the connected components of type $(y, 2)$ points and its relative boundary which is the
61 union of relative open (connected) edges formed by type $(z, 1)$ points and are type $(n, 0)$ points which we call the nodes of the
62 cell.

63 The definition of a closed 3-cell is analogous to the definition of a closed polyhedron which is the disjoint union of its open
64 faces.

65 **Definition 4** We call M a polyhedral tiling if, in $d = 2$ dimensions we have $x = 1, y = 2, n > 2$ and in $d = 3$ dimensions
66 we have $x = 1, y = 2, z > 2, n > 3$. We also require that all faces are C^2 -smooth 2-manifolds and all edges are C^2 -smooth
67 1-manifolds. Each edge connects exactly two nodes which we call the endpoints of the edge and in these nodes there are uniquely
68 defined half-tangents of the edges.

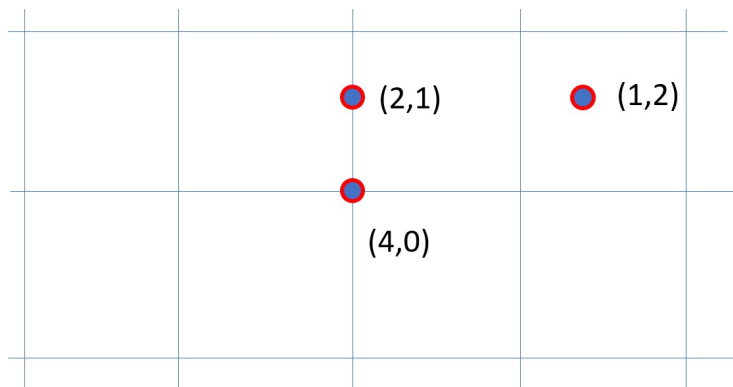


Fig. S1. Point types in 2 dimensions, illustrated on rectangular grid.. Interior of cell: $(1, 2)$; edge: $(2, 1)$; node: $(4, 0)$.

69 Obviously, polyhedral tilings contain polyhedral tilings as special cases. However, cells in polyhedral tilings may have curved
70 faces and edges. The fundamental concepts in the mean-field theory of mosaics (3, 4) are the cell and nodal degrees which we
71 define below.

72 **Definition 5** The combinatorial degree v of a cell in a polyhedral tiling is equal to the number of nodes at its boundary. We
73 refer to these nodes as the vertices of the cell. The combinatorial degree n of a node is equal to the number of cells overlapping
74 at that node. Alternatively, using Definition 4 we can say that if the type of the node is $(n, 0)$ then its combinatorial degree is n .

75 **Definition 6** We consider one vertex P of a cell c . We consider the edges belonging c , one endpoint of which is P and we
76 consider their half-tangents at P . We say that a vertex P of the cell c is sharp if there exists no pair among these different half
77 tangents which together form a straight line. If a vertex is not sharp then we say that it is a soft vertex with respect to c .

78 Using the concept of soft vertices we define the so-called corner degrees associated with cells and nodes. This definition is a
79 straightforward generalization of the definition given in (4).

80 **Definition 7** The corner degree v^* of a cell in a polyhedral tiling is equal to the number of its sharp vertices. The corner
81 degree n^* of a node is equal to the number of those cells sharp vertices meeting at that node in which this node is a sharp vertex.

82 **Definition 8** We call a node of a polyhedral tiling M a soft node if its corner degree can not be decreased by any local
83 homeomorphism that is a diffeomorphism constrained to the relative interior of the edges connecting at this node. We call M a
84 soft tiling if all of its nodes are soft. We call a cell a soft cell if it is the cell of a soft monohedric tiling.

85 Note that the concept of "soft node" is implicitly defined, so it is not easy to check whether a node is soft or not. Our goal
86 is to reduce the corner degree of a node, so we add local topological operations to make it "soft". Our intervention will be
87 successful if the final corner degree is zero.

88 **B. Definition of the edge bending algorithm.** Next we introduce the *edge bending algorithm* which, via a basic softening
89 operation transforms polyhedral nodes into soft nodes. Here we give a detailed mathematical description of the edge bending
90 algorithm the essence of which is also illustrated in Supplementary Movie SM1.

91 Let V be a node of the tile and let \mathcal{V} be the shape of a vertex figure containing the edges of the tiling whose one end is V .
92 The small sphere $S(V, \varepsilon)$ around V intersects \mathcal{V} in the vertex set of a convex polyhedron P inscribed in $S(V, \varepsilon)$, whose radial
93 projection from V is a convex tiling of the sphere. The faces of the spherical tiling correspond on the one hand to the faces

94 of P and on the other hand those 3-dimensional Q_k tiles of the tiling, which contains the vertex V . A spherical edge of a
 95 spherical tile corresponds to the common face $F_{k,l}$ of the tiles Q_k, Q_l . Note that all spherical tiles are also spherical convex
 96 and their union form a spherical edge-to-edge tiling. If the vertex set of P is $V(P) := \{w_1, \dots, w_\sigma\}$ and $e = (w_i, w_j)$ is an edge
 97 of P , then $e_{i,j}(V)$ represents the corresponding circular sector of the ball $B(V, \varepsilon)$, which is the convex hull of the segments
 98 $w_i V, V w_j$ and the spherical circular arc $w_i w_j$.

99 **Definition 9** We say that a node V can be completely softened if there is a homeomorphism $\Phi : B(V, \varepsilon) \rightarrow B(V, \varepsilon)$ that has
 100 the following properties:

101 i: $\Phi(x) = x$ if $x \in S(V, \varepsilon)$,

102 ii: Φ restricted to the relative interior of an edge of the vertex figure is a diffeomorphism,

103 iii: the semi-tangent line $\tau^+(w_i V)$ of the curve $\Phi(w_i V)$ at V for all vertices $w_i \in V(P)$ are on a fixed line $t = t^+ \cup \{V\} \cup t^-$
 104 through V ,

105 iv: and if the vertices w_{i_1}, \dots, w_{i_v} form a face of P then there are indices $i_k \neq i_l$ such that $\tau^+(w_{i_k} V) = t^+$ and $\tau^+(w_{i_l} V) = t^-$.

106 The geometric meaning of the definition is as follows. The node V can be completely softened if the edges in a small
 107 neighborhood of its vertex shape can be modified locally so that the 3-dimensional tiles meeting at V lose their corners without
 108 changing the global combinatorial structure. This requires that the circular sectors under the transformation do not cross each
 109 other, and in each spherical tile we find two vertices w_{i_k} and w_{i_l} , for which the corresponding curves $\Phi(w_{i_k} V)$ and $\Phi(w_{i_l} V)$
 110 touch the fixed line t from opposite directions.

111 C. The general combinatorial condition for node softening: Lemma 1 and its proof.

112 **Lemma 1** Let P denote a vertex polyhedron of a polyhedral tiling. Suppose that the vertices of P can be colored in such a way
 113 that the following two requirements are met:

114 • Each face has vertices colored with a different color.

115 • One of the two sub-graphs defined by coloring is edge-connected.

116 Then the node V can be completely softened.

117 **Proof:** First, choose a line $t = t^+ \cup \{V\} \cup t^-$ through V such that the planes (tw_i) are all distinct. (Consequently, $t \cap S(V, \varepsilon) \neq w_i$
 118 holds for all i .) Let t be the "vertical" line and let t^- be its half-line belonging to the lower hemisphere of $B(V, \varepsilon)$. Let N be
 119 the intersection of t^+ and $S(V, \varepsilon)$ (the north pole of the sphere) and let M be the opposite (south) pole of $S(V, \varepsilon)$. Then the
 120 circular sectors defined by the edges of the spherical polygons are transversal to the planes tw_i belonging to the end points of
 121 the edge. We keep these planes as the osculating planes of the image curves $\Phi(w_i V)$.

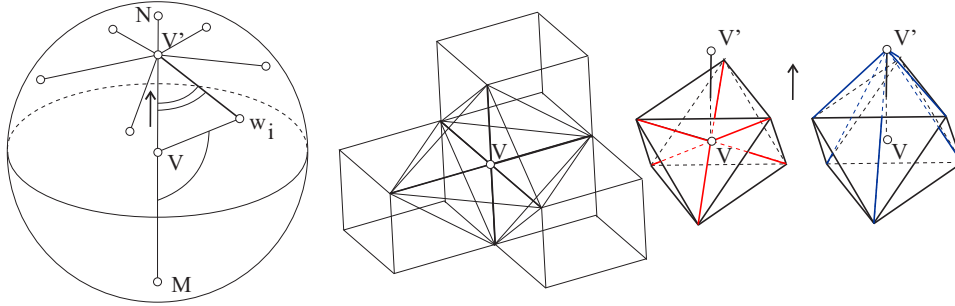


Fig. S2. On the left side, we can see the result of the lifting process with respect to the vertices w_i . A standard cubic tile has an octahedral vertex shape at any vertex. The effect of the lifting process can be seen in the two figures on the left. Red edges change to blue.

122 Secondly, we move the node V to the position V' of the segment \overline{VN} in such a way that the following conditions are met in
 123 the system:

- 124 • the union of the segments $\overline{V'X}$, where X runs along the points of the spherical edges, forms the same combinatorial
 125 decomposition of the interior of the ball $B(V, \varepsilon)$ as the original circular sectors,
- 126 • all $MV'w_i \angle$ angles should be acute angles.

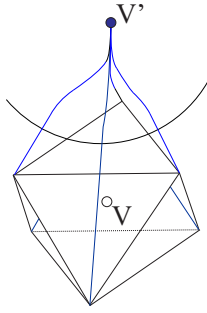


Fig. S3. In the "compression" step we change the straight segments of edges and flat parts of faces to suitable curves and surfaces.

127 Such a point V' exists because P is convex and N in the vertical direction lies higher than any vertex w_i . The result of this
128 "lifting process" can be seen on Fig.S2.

129 In the third step, we continuously deform the $w_k V' w_l$ sectors in a $B(V', \frac{\varepsilon}{2})$ sphere. Two things must be fulfilled in the end
130 of this step, the new surfaces must be tangentially connected to the sector part outside of this sphere, and the semi-tangents of
131 the new $w_i V'$ curves in V' must point in the $\overrightarrow{VV'}$ direction. This local transformation is called "compression". See in Fig.S3.

132 After this step, each new tile will have a vertex with zero solid angle at V' . In a tile T , at least three edges connect to each
133 other at V' , and for the sake of simplicity, we denote them again by $V' w_{i_k}$. If at least one, but not all, of the above edges of a
134 tile T with vertex V' can be "bend back" without changing the entire combinatorics, then in T we deleted V' from its corner,
135 since its two edges running into V' form a smooth curve. Our last step which we call "bending back of the edges" is the step by
136 step bending back of certain edges.

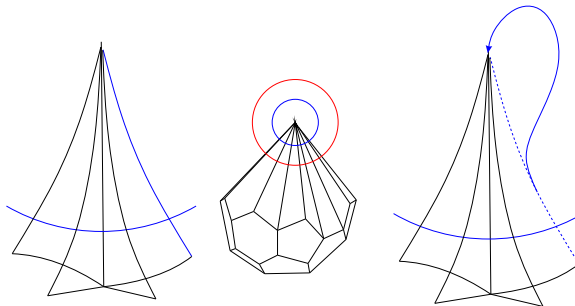


Fig. S4. In the "bending back" step we bend back an edge in a corner of a tile at V' .

137 The problem is that the process "bending back" requires "enough space". Since we do not want to change the combinatorics
138 of the vertex figure, the space required for bending back must be provided step by step. Before performing these steps, we see
139 a polyhedral graph on a smaller sphere $S(V', \frac{\varepsilon}{2})$ whose nodes and edges represent the original $V' w_i$ edges and central sector
140 surfaces. The latter divide the interior of the ball $B(V', \frac{\varepsilon}{2})$ according to the cell ranges. As usual, the resulting spherical graph
141 has a planar representation, where one face is the exterior of a convex polygon and the other faces derive a filling of the domain
142 of the polygon. As shown in Figure S5, the vertices of the outer surface correspond to bendable edges, but the edge belonging
143 to the inner vertex w_i can be bent if and only if there is a bent back vertex w_j for which $w_i w_j$ is an edge of the graph.

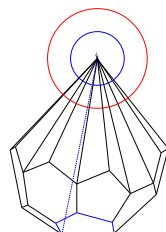


Fig. S5. The edges correspond to the vertices of the blue face cannot bent back if there is no bent back edge from the edges corresponding to the vertices of the outer face.

144 According to our condition for the graph, backbent and non-backbent edges can be divided into two sets, of which the set of
145 back bend edges (which we denote by \mathcal{A}) must be connected. In order to show that without changing the combinatorics of the

146 spherical tiling, we can really bend back the edges belonging to the vertex set \mathcal{A} , we describe the algorithm. Let the diameter
 147 d_1 of the first bend be the diameter of the convex hull of the curve $w_1 w_i \cap B(V', \frac{\varepsilon}{4})$.

148 STEP A: Consider the subgraph \mathcal{A} of vertices belonging to backbent edges. Let $w_1 \in \mathcal{A}$ be the vertex of the outer polygon,
 149 and replace the edges of \mathcal{A} with two edges of weight 1 in opposite directions.

150 STEP B: Find the minimal path of the obtained directed weighted graph for each pair of vertices $\{w_1, w_k\}$. The union of
 151 these paths is a spanning tree of the graph \mathcal{A} in which there is exactly one path from w_1 to every other vertex.

152 STEP C: Renumber the vertices of \mathcal{A} so that if there is an edge between w_i and w_j , then $i < j$ is also satisfied. Let the
 153 weight $u(i)$ of the vertex w_i be the number of edges in the path from w_1 to w_i . Finally, we define the width of the bending of
 154 the edge in w_i with the formula $d_i = \frac{d_1}{u(i)}$.

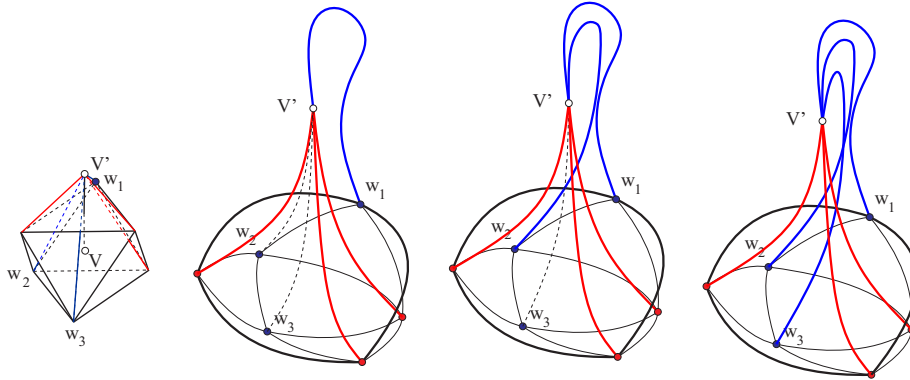


Fig. S6. Softening an octahedral vertex figure step by step

155 In Figure S6, we can see a complete process and the final result of the algorithm in the case where P is an octahedron. \square

156 **D. An easy-to-check sufficient condition for node softening: proof of Theorem 1.** Lemma 1 establishes a general (necessary
 157 and sufficient) condition under which a node can be completely softened. However, this condition is not easy to check or verify
 158 on a given node or on a given tiling. Our goal is to turn the combinatorial coloring condition of Lemma 1 into a much simpler
 159 statement of Theorem 1 about the existence of Hamiltonian cycles and paths on the dual of the vertex polyhedron.

160 Before establishing the link between coloring and Hamiltonian cycles, we first formulate a conjecture for the general case.
 161 The coloring condition can be formulated about the edge-vertex graph of the vertex polyhedron of a node. Since the node is
 162 combinatorially equivalent to a convex polytope inscribed in a sphere, our conjecture can be formulated as follows.

163 **Conjecture 1** *If Γ is a polyhedral graph then its vertices can be colored with two colors such that:*

164 *A: Each face has vertices colored with a different color.*

165 *B: One of the two monochromatic graphs defined by coloring is edge-connected in Γ .*

166 We only have partial results for this conjecture. A polyhedral graph (which is a 3-connected planar graph) always has a dual
 167 graph which is also 3-connected and planar. For simplicity, we use the notation \bar{e} for the edge of the dual graph corresponding
 168 to the edge e of the graph Γ . (It is clear that every edge in the polyhedral graph is also a common edge of two faces, so it
 169 corresponds to an edge of the dual graph.) We denote by $v(\Gamma)$, $e(\Gamma)$ and $f(\Gamma)$ the set of vertices, the set of edges and the set of
 170 faces of the graph Γ .

171 If G is a subgraph of Γ , then $\Gamma \setminus G$ is the graph that completes G with respect to Γ , containing those edges of Γ (and their
 172 endpoints) that are not in G . $G^* := (\Gamma \setminus G)^*$ denotes the dual of G with respect to Γ . Therefore Conj. 1 can be translated into
 173 the language of the dual graph as follows:

174 We look for the partition of the faces of the dual graph into two sets, such that every vertex of the graph belongs to a face
 175 of both sets, and one of the two sets is edge-connected. The next proposition is immediate.

176 **Proposition 1** *If the dual Γ^* of Γ is Hamiltonian (so it has a Hamiltonian cycle) then the statement of Conj. 1 is true.*

177 Indeed, if a dual graph has a Hamiltonian cycle, it defines two non-empty sets of faces on its "two sides" that satisfy the
 178 requirement properties. We note that in this case both of the sets are also edge connected. From the interesting counterexamples
 179 to Tait's conjecture by Tutte and others (see e.g. (5, 6)), we know that even a simple (or cubic) graph Γ^* can be non-Hamiltonian.
 180 Thus, even in the case where Γ is simple, our coloring problem is open. The following statement shows that the Hamiltonian
 181 property of a dual graph in the case of simple graphs can be weakened to the existence of a Hamiltonian path. (Such a graph is
 182 called traceable.)

183 **Proposition 2** *If the dual Γ^* of Γ is simple and traceable then the statement of Conj. 1 is true.*

Proof: Denote the elements of the Hamiltonian path of Γ^* by F_1, \dots, F_l which are triangles in Γ . The intersection of F_1 and F_2 is the edge $e_1 \in e(\Gamma)$ with vertices $v_1^1, v_1^2 \in v(\Gamma)$. We mark the vertices v_1^1 and v_1^2 with red and blue, respectively. The third vertex of F_2 is v_1^3 , so $F_2 \cap F_3$ is one of the edges $[v_1^1, v_1^3]$ or $[v_1^2, v_1^3]$. Denote this common edge by e_2 and color the vertex v_1^3 blue if $e_2 = [v_1^1, v_1^3]$ and red if $e_2 = [v_1^2, v_1^3]$. After that, consider e_3 , the next element of the path, which is the intersection of F_3 and F_4 . Since the vertices of the edge $e_2 = F_2 \cap F_3$ are colored, the color of the third vertex v_2^3 of the face F_3 should be different from the color of the other vertex of the new edge e_3 . Continuing the procedure, it can be seen that at a new step, one set of colored vertices does not change, and the other one gets a vertex connected by an additional edge, so the connectivity of this set still exists. Since each face contains at least one edge $e_i \in e(\Gamma)$, which is also an edge of the Hamiltonian path, and two vertices of such an edge are colored with two different colors, each face has vertices colored with different colors. The procedure also guarantees that the two sets of single-color vertices will be edge-connected in Γ , as we already mentioned. \square

Remark 1 Since a complete graph with four vertices has a Hamiltonian cycle, any simple graph that is recursively defined from it by turning a vertex into a triangular face also has this property. Indeed, if the degree of the vertex v to be omitted is three, a Hamilton circuit uses exactly two of the incoming edges, let them be \bar{e}_1 and \bar{e}_2 . At the same time as omitting v , we add three other vertices labeled v_1, v_2, v_3 to the graph, which match the edges $\bar{e}_1, \bar{e}_2, \bar{e}_3$ running into v . We drop the segments $[v_i, v]$ from the edges e_i and add three new edges $\bar{e}'_i = [v_j, v_k]$ to the graph. The part $\bar{e}_1 v \bar{e}_2$ of the original Hamilton circuit can be changed to the path $\bar{e}_1 v_1 \bar{e}'_2 v_3 \bar{e}'_1 v_2$, replacing the old Hamilton circuit with a new one.

Note that at each step a Hamiltonian path can be expanded in this way into a Hamiltonian path of the extended graph. So, by augmenting the graph Γ by replacing one triangular face with three other triangular faces that contain a new node, the traceability property of the dual graph Γ^* is not damaged. The number of vertices, edges, and faces of Γ increases by 1, 3, and 2 per step.

With the above assertions, if Γ is such a triangulated graph (or triangulation) that is dual with the Hamiltonian property (the existence of a path or a cycle), then we can produce a "good" coloring of the vertices such that both the monochromatic parts are edge-connected. The reverse of this statement is also true.

Proposition 3 In the case of triangular graphs the properties

A Each face has vertices colored with a different color.

C Both monochromatic parts of the vertices are edge-connected with respect to Γ .

together is equivalent to the traceability of its simple dual.

Proof: The existence of a Hamiltonian path H in Γ^* is equivalent to the property that there is a spanning tree T in Γ such that every face of Γ contains at least one edge of the edges of T . Indeed, by the definition of a path, H is a tree in Γ^* , which means that the dual of its complement $(\Gamma^* \setminus H)^*$ is a T tree in Γ . Since the degree of a vertex $F \in v(\Gamma^*)$ of H is at most 2, and the corresponding face $F \in f(\Gamma)$ has precisely three edges, at least one of them is an edge of T , too. (More precisely, there are exactly two faces in Γ that have only one edge from T , the other faces contain two edges from the edges of T .) The algorithm for proving Prop.2, under the assumption of the existence of such a T tree, can be applied to triangulation, i.e. the vertices of Γ can be colored with two colors so that properties [A] and [C] both hold.

Therefore, we now only need to prove that if the vertices of a triangulation Γ can be colored with two colors such that the coloring has the properties [A] and [C], then there is a spanning tree T of Γ such that each face contains at least one edge of T . Note that the monochromatic parts must be trees, because if there is a monochromatic cycle, then the third vertex of the two triangles defined by one of its edges has a different color than the color of the vertices belonging to the cycle. Since we colored with two colors, these two vertices have the same color. Due to the simple connectivity of the graph, these two monochromatic vertices are separated by the given cycle, which contradicts the connectivity condition for this color. Let the tree T be the union of these monochromatic trees connected by an extra edge. Since every face contains an edge with vertices of the same color, T also has the desired property. \square

Remark 2 According to the above, [A] and [B] give a weaker condition for a polyhedral graph with triangular faces than if we assume the existence of the Hamilton path for the dual. Thus, the class of simple graphs whose dual satisfies the conditions [A] and [B], contains the class of traceable simple polyhedral graphs.

Finally, we prove Theorem 1:

Proof: [Proof of Theorem 1.] The nodes in a normal, balanced tiling with the existence of the described limits form a discrete point system with finite number of combinatorial types. The nodes in a type can be softened parallel with the same steps, and we assume that at the same moment. Since each node have a neighbour which doesn't contains another one, we can soften the nodes of distinct types independently. The combinatorial condition in Lemma 1 by Proposition 1 holds, hence it can be applied. This proves the statement. \square

2. Analytical examples of soft monohedrally tilings

In the previous sections, we saw that polyhedral tilings the vertex figures of which meet certain combinatorial conditions can, in principle be deformed into soft tilings by using local changes. In this section, we perform this algorithm on some prismatic monohedral tilings to obtain soft, monohedrally tilings.

239 **Monohedral convex prismatic tilings of \mathbb{R}^3 .**

240 **Definition 10** A tiling of a space is *prismatic* if there are a finite number of infinite prisms whose non-overlapping congruent
241 copies fill the space. A *prismatic tiling* is *monohedral* if all prisms are congruent. A monohedral prismatic tiling is *convex* if the
242 prototype cell is a convex infinite prism.

243 **Proposition 4** Suppose that the three-space is filled by infinite prisms of finite type. Then the edges of the prisms are parallel
244 to a given plane.

245 **Proof:** Consider a prism P and one of its faces F . The plane H contains F , and the half-space H^+ bounded by H contains P .
246 Clearly, F is an infinite strip in H and must be covered by prisms of the tiling that lie completely in the complementary closed
247 half-space $H \cup H^-$. Since a half-space only contains infinite prisms whose edges are parallel to the boundary plane, we have
248 two options for covering the strip. Or F can be covered with a finite number of prisms whose edges are parallel to the edges of
249 P ; or F is covered by a countable set $\mathcal{Q} = Q_i : i \in N$ of parallel prisms whose suitable faces intersect F . In the latter case,
250 $\cup \mathcal{Q}$ also covers the entire plane H (cutting the space into two parts), and the edges of each additional prism R must also be
251 parallel to the plane H (see Fig. S7).

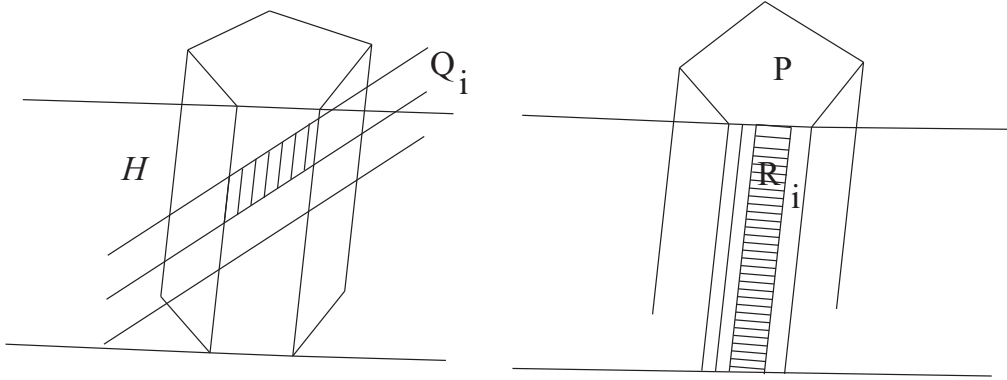


Fig. S7. The two possibilities to cover the face F of a prism.

252 We now consider the first case. The entire face $F_1 := F$ must be covered by parallel prisms $R_i \subset H^-$, $i = 1, \dots, k$, so one
253 edge e_1 of F_1 also belongs to a prism R_k . On the other hand, if we consider the other face of F_2 of P containing e_1 , we can
254 apply the above idea and see that either the plane of F_2 can be covered with an infinite number of intersecting prisms of type
255 Q_i , or a finite number of prisms R_{k+1}, \dots, R_{k+l} with an edge parallel to e_1 cover F_2 (see Fig. S8).

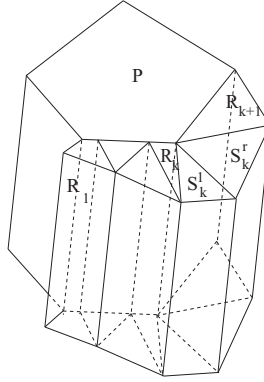


Fig. S8. The crown of the original prism

256 It is possible that already three columns P, R_k and R_{k+1} form the complete 3-dimensional neighborhood of the edge e_1 , so
257 that R_k and R_{k+1} has a common face containing e_1 , but this may not be the case. Now consider the face G of column R_k
258 that contains e_1 but does not lie in H and apply the above discussion to it. Either we end up with a fully covered plane and
259 the process is finished, or we get a new prism S_k^l that contains e_1 and shares a face with R_k . Since we have a finite number of
260 separate (non-congruent) prisms, we finally find a finite number of S_k^1, \dots, S_k^r prisms, with which $P, R_k, S_k^1, \dots, S_k^r, R_{k+1}$ prism
261 sequence gives the entire neighborhood of edge e_1 . Considering the next face F_3 of P and continuing the process, we can
262 specify the set of prisms that form the entire neighborhood of P (in the filling, this is the so-called crown of P). Since we
263 started from an existing filling, the process can be continued, and either we find a plane with which the edge of each tile is
264 parallel, or specifically, each prism is parallel to the starting prism P . This proves the claim. \square

265 **Remark 3** Note that if we tile a strip of space with parallel prisms, we can arbitrarily rotate it about a line perpendicular
 266 to the parallel planes of the strip. We can make a complete tile from such strips (broken into prisms). Thus, the result of
 267 the statement is sharp. When we examine monohedral tilings and observe that the tiling has an infinite prototile, which is
 268 an infinite prism, we concentrate only one possible tiling of the prototile prism. We do not search for all possible prismatic
 269 non-equivalent tilings, with the given prototype.

270 **A. The soft tetrahedral space-filler.** A space-filling polyhedron is one whose replicas can be packed so that these replicas
 271 completely fill the three spaces. To this day, we only know partial answers to the question posed by Hilbert in the eighteenth
 272 problem: "Which are the polyhedra with which we can completely fill the space by placing congruent copies next to each
 273 other?" The general answer to the question about tetrahedra is still unknown, but we know some non-trivial tetrahedral space
 274 fillers from the long literature of the problem. A good overview of the corresponding results can be found in Goldberg (7).
 275 Among these tetrahedral space fillers, we choose one that creates a prismatic monohedral filling with a screw movement. This
 can be seen in Fig. S9. In this filling, the union of three tetrahedra (namely, $ABCD$, $BCDE$, and $CDEF$) forms a triangular

THREE INFINITE FAMILIES OF TETRAHEDRAL SPACE-FILLERS

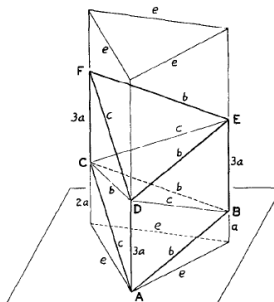


FIG. 2. Derivation of first infinite family.

Fig. S9. Goldberg's construction of spacefilling tetrahedra (7)

276 skew-prism $ABCDEF$. Therefore, we can fill an infinite prism with appropriate shifts in the direction of the AD edge. Since
 277 the orthogonal cross-section of the above infinite prism is a regular triangle, arbitrary tiling of the plane with congruent,
 278 equilateral triangles defines also a prismatic tiling of the space. That is, we can fill the space with congruent copies of the
 279 $ABCD$ tetrahedron.
 280

From the prototype of the tetrahedral space filler, we can create a curvilinear tetrahedron, which has no apex in the classical
 281 geometric sense. The result is a polyhedric and soft tiling according to the definitions 4 and 8. Thus, the tile cell is also soft,
 282 with one straight edge and five curved edges. It has two curved and two flat faces, the curved and flat faces are congruent in
 283 pairs. The common edge of the flat faces is straight, and the angle of these faces is sixty degrees. The "lower" curved face
 284 (which is the lower one in S10) can be moved to the top with a screw movement.

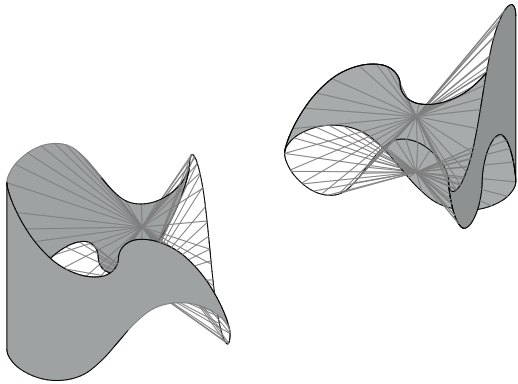


Fig. S10. The picture shows a tetrahedral space-filler without vertices

286 In the following, we give the analytical description of the vertex-less space-filling "tetrahedron". The parametric formulas of
 287 the curvilinear edges $AB = \gamma_1$, $BC = \gamma_2$ and $CA = \gamma_3$ of the lower face are given by the following formulas:

$$\gamma_1(\varphi) = \begin{cases} \left(-\frac{3}{4}(\cos \varphi + 1) + \frac{1}{2}, -\frac{\sqrt{3}}{4}(\cos \varphi + 1) - \frac{\sqrt{3}}{2}, -\frac{1}{4}(\cos \varphi + 1) + \frac{\sqrt{3}}{2} \sin \varphi\right), & 0 \leq \varphi \leq \pi \\ \left(\frac{3}{4}(\cos \varphi + 1) + \frac{1}{2}, \frac{\sqrt{3}}{4}(\cos \varphi + 1) - \frac{\sqrt{3}}{2}, \frac{1}{4}(\cos \varphi + 1) + \frac{\sqrt{3}}{2} \sin \varphi\right), & \pi \leq \varphi \leq 2\pi \end{cases} \quad [1]$$

289

$$\gamma_2(\varphi) = \begin{cases} (\frac{3}{4}(\cos \varphi + 1) + \frac{1}{2}, -\frac{\sqrt{3}}{4}(\cos \varphi + 1) + \frac{\sqrt{3}}{2}, -\frac{1}{4}(\cos \varphi + 1) + \frac{\sqrt{3}}{2} \sin \varphi + 1), 0 \leq \varphi \leq \pi \\ (-\frac{3}{4}(\cos \varphi + 1) + \frac{1}{2}, \frac{\sqrt{3}}{4}(\cos \varphi + 1) + \frac{\sqrt{3}}{2}, \frac{1}{4}(\cos \varphi + 1) + \frac{\sqrt{3}}{2} \sin \varphi + 1), \pi \leq \varphi \leq 2\pi. \end{cases} \quad [2]$$

290

$$\gamma_3(\varphi) = \begin{cases} (-1, \frac{\sqrt{3}}{2}(\cos \varphi + 1), \frac{1}{2}(\cos \varphi + 1) + \frac{\sqrt{3}}{2} \sin \varphi + \frac{1}{2}), 0 \leq \varphi \leq \pi \\ (-1, -\frac{\sqrt{3}}{2}(\cos \varphi + 1), -\frac{1}{2}(\cos \varphi + 1) + \frac{\sqrt{3}}{2} \sin \varphi + \frac{1}{2}), \pi \leq \varphi \leq 2\pi. \end{cases} \quad [3]$$

291 We define the closed leading curve Γ as the union of these curves, so $\Gamma = \gamma_1 \cup \gamma_2 \cup \gamma_3$. Let the centroid $S = (0, 0, 1/2)$ of the
292 point set $\{A, B, C\}$ be the vertex of the surface. The conic surface fitted to the leading curve Γ can be given in the following
293 form:

294

$$r(\varphi, \psi) = (1 - \psi)(0, 0, 1/2) + \psi \Gamma \text{ where } 0 \leq \psi \leq 1. \quad [4]$$

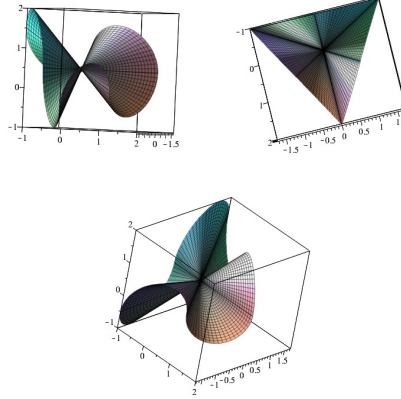


Fig. S11. Three views of the curved face of a soft tetrahedric cell

295 Note that the surface $r(\varphi, \psi)$ is not smooth at the point S , because the semitangents at these points do not fall in a common
296 plane. At the same time, in the metric sense, no edge passes through the point S , and S is not a vertex of the surface in
297 the combinatorial sense, because it contains exactly two cells. (In addition, the medians of the triangle ABC are also the
298 generators of the surface r .) Three views of this face are shown in Fig. S11.

Using quadratic (or higher order) Bezier curves (see e.g. (8)) we can immediately create smooth versions of this surface. Let the components (coordinate functions) of Γ be $\Gamma_1(\varphi), \Gamma_2(\varphi)$ and $\Gamma_3(\varphi)$. Denote this curve $T(\varphi) = (T_1(\varphi), T_2(\varphi), T_3(\varphi))$, where: $T_1(\varphi) = \frac{1}{2}\Gamma_1(\varphi), T_2(\varphi) = \frac{1}{2}\Gamma_2(\varphi)$ and $T_3(\varphi) = \frac{1}{2}$. Then, for a fixed φ , the quadratic Bezier curve is

$$B(\psi) = \psi^2 t_2 + 2\psi(1 - \psi)t_1 + (1 - \psi)^2 t_0$$

299 where $t_0 = S$, $t_1 = T(\varphi)$ and $t_2 = \Gamma(\varphi)$. It is a parabolic arc whose tangent at point S is horizontal. That's why the
300 corresponding surface $r_T(\varphi, \psi)$ is smooth at the point S with a horizontal tangent plane.

301

$$r_T(\varphi, \psi) = \psi^2 t_2 + 2\psi(1 - \psi)t_1 + (1 - \psi)^2 t_0 = \psi^2 \Gamma(\varphi) + 2\psi(1 - \psi)T(\varphi) + (1 - \psi)^2 S \quad [5]$$

There is also a simple description of this surface using coordinate functions, the summation in the first two components is simplified to $\psi^2 \Gamma_i + 2\psi(1 - \psi) \frac{\Gamma_i}{2} = \psi \Gamma_i$, while the third component takes the form $\psi^2 \Gamma_3 + (2\psi(1 - \psi) + (1 - \psi)^2) \frac{1}{2} = \psi^2 \Gamma_3 + (1 - \psi^2) \frac{1}{2}$. So the smooth surface generated by the curve $T(\varphi)$ is

$$r_T(\varphi, \psi) = \left(\psi \Gamma_1(\varphi), \psi \Gamma_2(\varphi), \psi^2 \Gamma_3(\varphi) + \frac{1 - \psi^2}{2} \right).$$

302 On Fig. S12 we can see three view of this surface.

303 Finally, apply a screw movement in the direction of the z axis, with a distance of $4m = 1$ and a rotation angle of $2\pi/3$. The
304 constructed ABC face is moved to another position with the rule: Images of A, B and C are B, C and $D = (-1, -\sqrt{3}, 5/2)$.
305 These two surfaces have a common curvilinear edge BC . From the infinite prism above the regular triangle PQR , the surfaces
306 ABC and BCD intersect a region with a tetrahedral combinatorics, whose planar faces are shown in Fig. S13. From Goldberg's
307 original construction, it is easy to see that the above screw displacement moves the $ABCD$ tetrahedral domain into another
308 $BCDE$ tetrahedral domain, which has BCD as its common face with the first one. Applying the same screw movement, we
309 obtain a third copy of $CDEF$ that matches the previous ones. The union of the three tetrahedral domains is a prism whose
310 faces ABC and DEF are translates of each other. With such congruent prisms, the space can be filled according to the original
311 construction. We get that $ABCD$ is a soft space-filling cell with tetrahedral combinatorics.

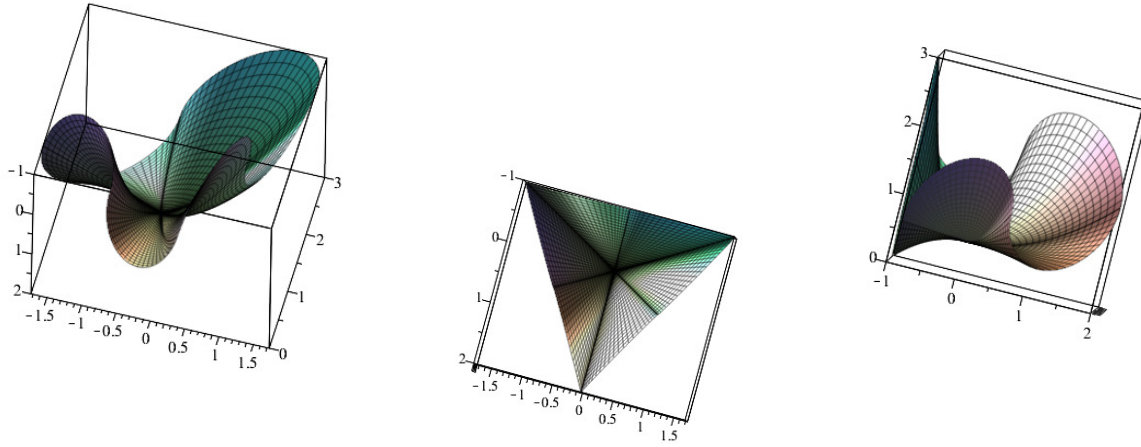


Fig. S12. The smooth curvilinear face of the space-filling soft "tetrahedron".

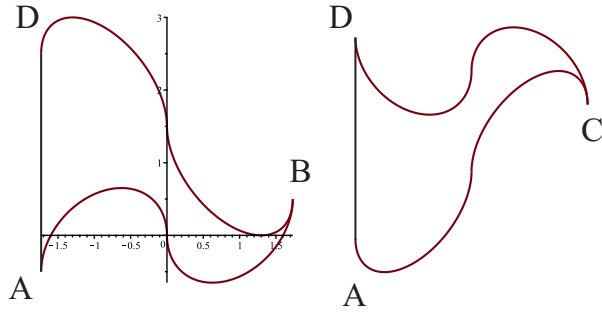


Fig. S13. Planar faces of the soft "tetrahedron".

312 **B. Prismatic monohedric tilings with rotational symmetries.** In this section, we provide additional soft monohedric tilings using
 313 the method of the previous subsection. If the normal section of the prismatic cell has rotational symmetry, then this section is
 314 a regular polygon. The fillability of the plane assumes three-, four-, or six-order symmetry, so we provide constructions for
 315 these possibilities.

316 **B.1. Triangular prism.** The straight edges of the prism are vertical and pass through $A(-1, -\sqrt{3}, 0)$, $B(2, 0, 0)$ and $C(-1, \sqrt{3}, 0)$
 317 points. The formulas for the edges of the lower curved surface are

$$\gamma_1(\varphi) := \begin{cases} \left(\frac{3}{4} \cos \varphi + \frac{5}{4}, \frac{\sqrt{3}}{4} \cos \varphi - \frac{\sqrt{3}}{4}, \frac{\sqrt{3}}{2} \sin \varphi\right) & 0 \leq \varphi \leq \pi \\ \left(-\frac{3}{4} \cos \varphi - \frac{1}{4}, -\frac{\sqrt{3}}{4} \cos \varphi - \frac{3\sqrt{3}}{4}, \frac{\sqrt{3}}{2} \sin \varphi\right) & \pi \leq \varphi \leq 2\pi \end{cases} \quad [6]$$

$$\gamma_2(\varphi) := \begin{cases} \left(-\frac{3}{4} \cos \varphi - \frac{1}{4}, \frac{\sqrt{3}}{4} \cos \varphi + \frac{3\sqrt{3}}{4}, \frac{\sqrt{3}}{2} \sin \varphi\right) & 0 \leq \varphi \leq \pi \\ \left(\frac{3}{4} \cos \varphi + \frac{5}{4}, -\frac{\sqrt{3}}{4} \cos \varphi + \frac{\sqrt{3}}{4}, \frac{\sqrt{3}}{2} \sin \varphi\right) & \pi \leq \varphi \leq 2\pi \end{cases} \quad [7]$$

$$\gamma_3(\varphi) := \begin{cases} \left(-1, -\frac{\sqrt{3}}{2} \cos \varphi - \frac{\sqrt{3}}{2}, \frac{\sqrt{3}}{2} \sin \varphi\right) & 0 \leq \varphi \leq \pi \\ \left(-1, \frac{\sqrt{3}}{2} \cos \varphi + \frac{\sqrt{3}}{2}, \frac{\sqrt{3}}{2} \sin \varphi\right) & \pi \leq \varphi \leq 2\pi \end{cases} \quad [8]$$

The union $\Gamma = \gamma_1 \cup \gamma_2 \cup \gamma_3 = (\Gamma_1, \Gamma_2, \Gamma_3)$ gives the leading curve the curved faces which we construct with Bezier's method.
 Now we have

$$T(\varphi) = \left(\frac{1}{2}\Gamma_1(\varphi), \frac{1}{2}\Gamma_2(\varphi), 0\right)$$

323 and

$$r_T(\varphi, \psi) = 2\psi(1-\psi)T(\varphi) + (1-\psi)^2 T(\varphi) = ((1-\psi)\Gamma_1, (1-\psi)\Gamma_2, (1-\psi)^2 \Gamma_3), \quad [9]$$

324 because the centroid is the origin. The translation of $r_T(\varphi, \psi)$ with the vector $(0, 0, 1)$ gives the second curved face, so the
 325 analytic description of the tile is:

$$K = \{r_T(\varphi, \psi) + (0, 0, z) \text{ where } 0 \leq z \leq 1\}. \quad [10]$$

326 We can see the parallel curved faces in Fig. S14.

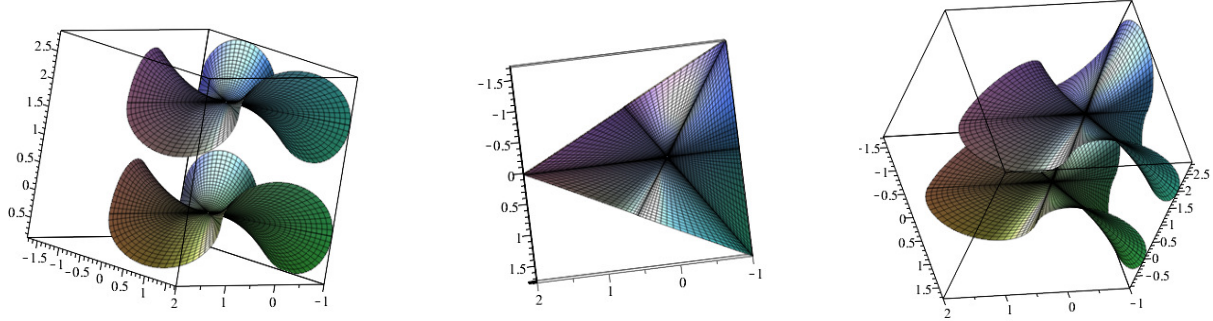


Fig. S14. Three views of the soft triangular prismatic tile.

329 **B.2. Squared prism.** Our previous paper (4) contains a simple example (see Fig. 4 therein) with curved faces $z = \sqrt{(1-x^2)} -$
 330 $\sqrt{(1-y^2)} \pm 1$.

331 **B.3. Hexagonal prism.** The method of paragraph B.1 can be used to analytically construct a hexagonal prism. Edge curves can
 332 be assembled from two parts, originated from the prototypes

$$333 \quad \gamma'(\varphi) := \left(\frac{\sqrt{3}}{2} \cos \varphi + \frac{\sqrt{3}}{2}, 0, \frac{\sqrt{3}}{2} \sin \varphi \right) \quad \text{if } 0 \leq \varphi \leq \pi \quad [11]$$

$$334 \quad \gamma''(\varphi) := \left(-\frac{\sqrt{3}}{2} \cos \varphi - \frac{\sqrt{3}}{2}, 0, \frac{\sqrt{3}}{2} \sin \varphi \right) \quad \text{if } \pi \leq \varphi \leq 2\pi. \quad [12]$$

335 In the present case the prototype γ' have to fit to the 1th, 3th and 5th edges of a regular hexagon getting γ'_1 , γ'_2 and γ'_3 ,
 336 respectively, and the prototype γ'' can be fitted to the 2th, 4th and 6th edges of the hexagon giving the curves γ''_i .

337 3. Additional geometric concepts

338 **A. The geometry of z-cells.** Here we give formal, detailed definition of z-cells which aims not only to characterize their geometry
 339 but also provide an algorithm for their construction.

340 **Definition 11** Let b_0 be a simple planar closed curve in the $[xy]$ plane. From b_0 , we build an infinite solid prism B by
 341 translating b_0 and its interior along the z direction and generating from each point on b_0 a one-parameter family f of lines
 342 parallel to the z -axis. Let Γ be the group which leaves the $[xy]$ sections of B invariant. Let M_1, M_2 be connected 2D manifolds,
 343 intersecting B in such a way that the respective simple, closed curves b_1, b_2 are disjoint and each of them has a single intersection
 344 point with each member of f . These intersections $\mathcal{M}_1 = M_1 \cap B$ and $\mathcal{M}_2 = M_2 \cap B$ are called full cuts. Let \mathcal{B} be the finite
 345 subset of B generated by the two full cuts. We call \mathcal{B} a z-cell if its copies fill B without overlaps and without gaps. We recognize
 346 some special cases:

- 347 1. If there exists a rigid body transformation $T : \mathcal{M}_1 \rightarrow \mathcal{M}_2$, then we call \mathcal{B} a primary z-cell.
- 348 2. If both b_1, b_2 are smooth then \mathcal{B} has no sharp corners and we call it a soft z-cell.
- 349 3. If b_0 is the boundary of a monomorphic cell and \mathcal{B} is a z-cell, then copies of \mathcal{B} fill 3D space without gaps and we call \mathcal{B} a
 350 spacefilling xyz-cell.
- 351 4. If \mathcal{B} is a spacefilling z-cell with $0 < v^* < 4$ then it is a softened spacefilling z-cell.
- 352 5. If \mathcal{B} is a spacefilling z-cell with $v^* = 0$ then it is a soft spacefilling z-cell

353 **Lemma 2** The necessary and sufficient condition for \mathcal{B} to be a primary z-cell is that $T = g \circ t$, where $g \in \Gamma$ and t is the unit
 354 translation in the z direction.

355 The proof of Lemma 2 is straightforward. We remark that non-primary z-cells can be obtained by suitable bisections of primary
 356 z-cells. A simple example of a primary soft z-cell is to take b_0 to be a circle in the $[xy]$ plane and take M_1 and M_2 to be
 357 distinct planes normal to the z -axis. Then, b_1 and b_2 are circles parallel to b_0 , \mathcal{M}_1 and \mathcal{M}_2 are disks and \mathcal{B} is a finite solid
 358 circular cylinder.

359 While soft spacefilling z-cells are just special cases of soft cells, they highlight the difficulty of such constructions: if the
 360 planar curve b_0 is smooth then it is easy to find M_1, M_2 such that b_1, b_2 are smooth and we have a soft z-cell, as in the previous

example of the solid circular cylinder. However, in this case this cell will be not filling 3D space. The balloon constructions of Seilacher (9) are yet another example of soft z -cells which, however, in general, are not filling 3D space. On the other hand, if b_0 is a 2D monomorphic cell then it can not be smooth and the manifolds M_1, M_2 resulting in smooth curves b_1, b_2 are nontrivial. If b_0 is non-smooth but b_1, b_2 are smooth then the latter will have inflectional tangencies in the z -direction at all edges.

B. The softness of rotational ellipsoids. We regard a rotational ellipsoid E_a with half axes $(a, 1, 1)$ with $a \in [0, 1]$ and our goal is to show that the rolling radius of this body is $\rho(E_a) = 1$. We imagine the half axis with length a to be aligned with the vertical y axis and we parameterize the meridian in the $[xy]$ plane by the central angle φ as

$$x = -\cos(\varphi), \quad y = a \sin(\varphi). \quad [13]$$

At the point $P(x(\varphi), y(\varphi))$ the radius r of the horizontal $[xz]$ section of E_a can be written as

$$r(\varphi) = |x| = \cos(\varphi), \quad [14]$$

and using the theorem of Meusnier we can write the radius R of the normal section (which is a principal section) as

$$R(\varphi) = r(\varphi)/\cos(\beta), \quad [15]$$

where β is the angle between the surface normal and the horizontal x axis. Let us differentiate with respect of φ :

$$\dot{x} = \sin(\varphi), \quad \dot{y} = a \cos(\varphi). \quad [16]$$

Now we can write

$$\cos(\beta) = \frac{\cos(\varphi)}{\sqrt{\frac{\sin^2(\varphi)}{a^2} + \cos^2(\varphi)}}, \quad [17]$$

so we have

$$R(\varphi) = \sqrt{\frac{\sin^2(\varphi)}{a^2} + \cos^2(\varphi)}. \quad [18]$$

If $a < 1$ then $R(\varphi) \geq 1$ and we have equality only at $\varphi = 0$ on the equator. This implies that for $a < 1, \varphi \neq 0$ at every point of the surface we have at least one section where the radius of curvature greater than one, so at any surface point P not lying on the equator for the rolling radius we have $\rho(P) > 1$. Since for the points of the equator we have $\rho(P) = 1$, the rolling radius of the ellipsoid is $\rho(E_a) = 1$. Since the surface area of the ellipsoid is a monotonically increasing function of a , so is the softness which assumes its maximum at $a = 0$ with $\sigma(E_0) = 1$ on the circular disc and at $a = 1$ with $\sigma(E_1) = 1/\sqrt{2}$ on the sphere.

If $a > 1$ then it is still true that the surface area is growing with a , however, the rolling radius is not constant any more but it is decreasing: at $\varphi = \pi/2$, $R(\varphi)$ has an extremum for every value for a , however, for $a < 1$ this is a maximum, so it does not influence the rolling radius but for $a > 1$ it is a minimum, so for $a > 1$ we have $\rho(E_a) = 1/a$. This implies that the softness $\sigma(E_a)$ is a monotonically decreasing function of the parameter a for any $a \geq 0$ and we have $\sigma(E_a) \rightarrow 0$ as $a \rightarrow \infty$.

388 4. Illustration of soft monohedral tilings

389 **A. Detailed illustration of the 7 soft cells shown in Figure 4, panels (d1-d4,f1-f3) of the main text.** In this subsection we expand
390 Figure 4 of the main text. First, in Figure (S15) we show details about the softness values associated with the 5 Dirichlet-Voronoi
391 cell, then, in Figures (S16)-(S22) we provide separate illustrations for each of the 7 soft cells shown in Figure 4. Each figure
392 shows both the original, spacefilling non-soft cell as well as the soft cell along with the image of the corresponding tiling.

	NON SOFT	SOFT	AREA	MIN. ROLLING RADIUS	SOFTNESS	MAX. SOFTNESS
CUBE			$A = 4h + 4.1514$	$\rho = 0.5$	$\sigma(h) = \frac{1}{2} \sqrt{\frac{2\pi}{4h+4.1514}}$	$\sigma_{max} = \sigma(0) = 0.615$
HEXAGONAL PRISM			$A = 6h + 9.39$	$\rho = 0.5$	$\sigma(h) = \frac{1}{2} \sqrt{\frac{2\pi}{6h+9.39}}$	$\sigma_{max} = \sigma(0) = 0.409$
ELONGATED DODECAHEDRON			$A = 29.796$	$\rho = 0.433$	$\sigma = 0.199$	
TRUNCATED OCTAHEDRON			$A = 22.367$	$\rho = 0.707$	$\sigma = 0.375$	
ROMBODODECAHEDRON			$A = 22.402$	$\rho = 0.408$	$\sigma = 0.216$	

Fig. S15. Softness values associated with the soft versions of the 5 Dirichlet-Voronoi cells shown in panels (d3),(d4),(f1),(f2),(f3) of the main text.

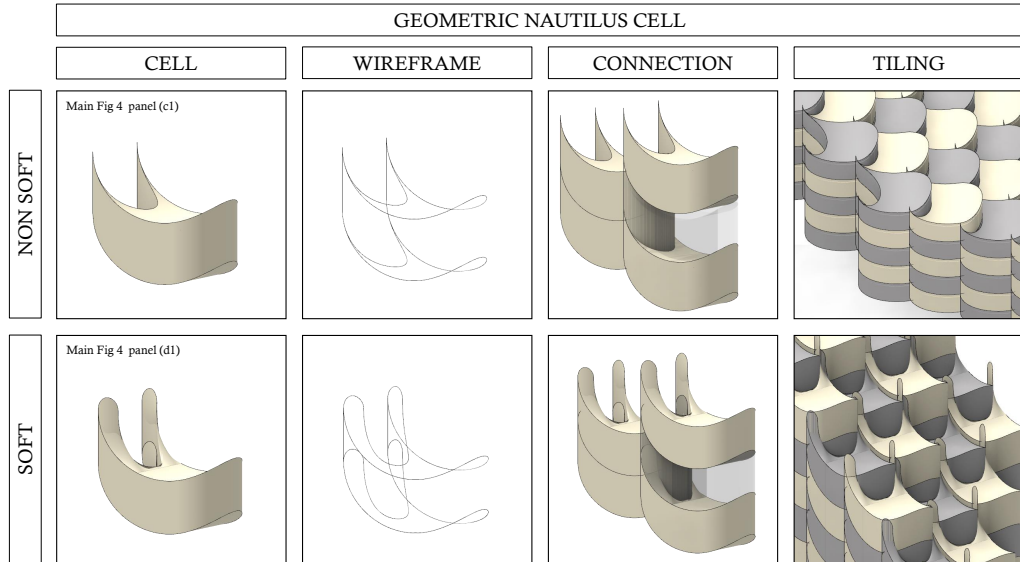


Fig. S16. The geometric Nautilus cell. Detailed views of the soft cell shown in Figure 4, panel (d1) of the main text. Upper row: geometry of the space-filling non-soft cell from which the soft cell was constructed. Lower row: geometry of the soft cell.

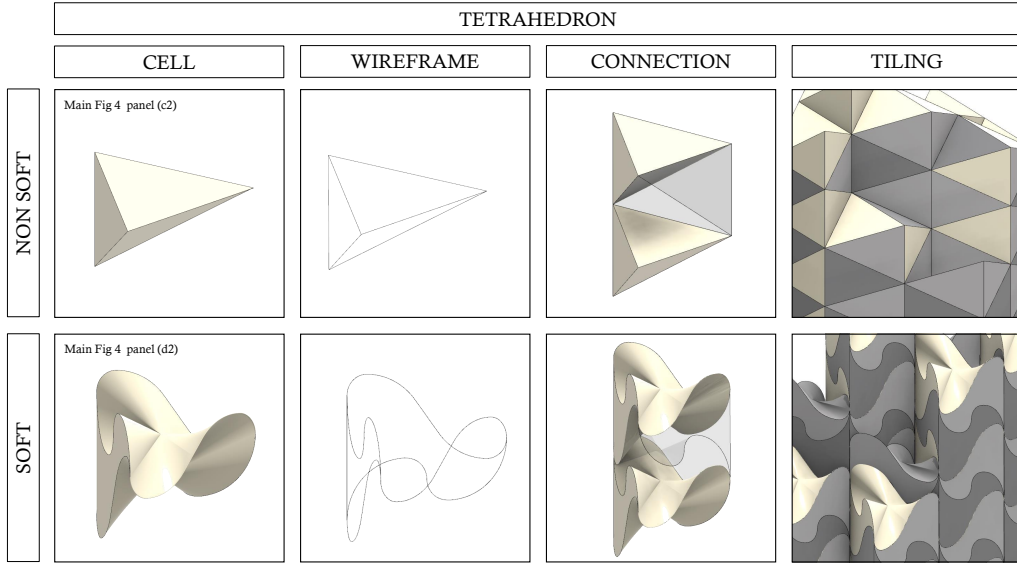


Fig. S17. The tetrahedron cell. Detailed views of the soft cell shown in Figure 4, panel (d2) of the main text. Upper row: geometry of the space-filling non-soft cell from which the soft cell was constructed. Lower row: geometry of the soft cell.

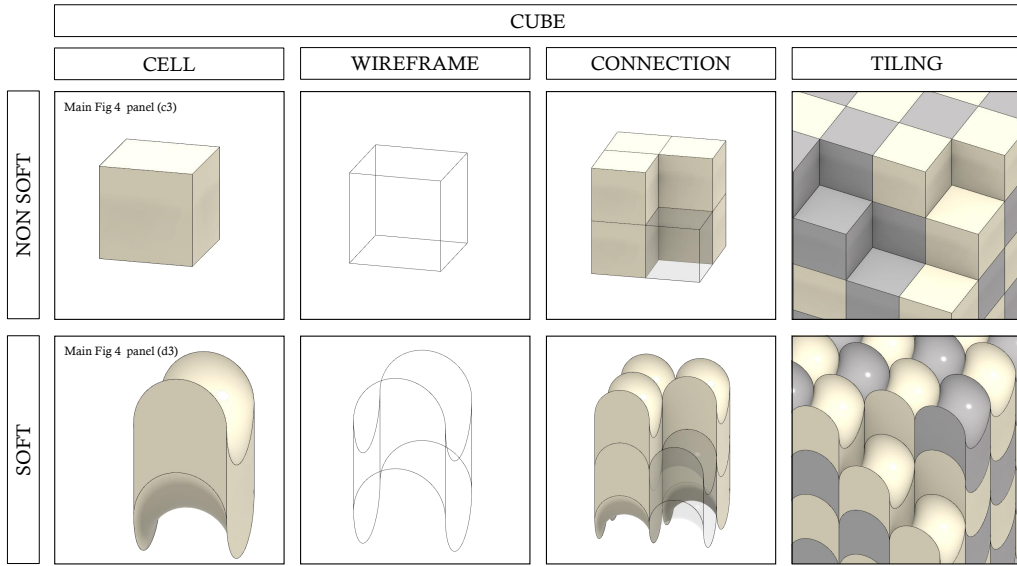


Fig. S18. The cube cell. Detailed views of the soft cell shown in Figure 4, panel (d3) of the main text. Upper row: geometry of the space-filling non-soft cell from which the soft cell was constructed. Lower row: geometry of the soft cell.

393 B. Soft cells appearing in art.

394 **B.1. Soft 3D cells in architectural design.** Beyond natural examples, the shape of soft monohedric cells also appears in architectural
 395 design. Figure S23 shows two such examples, associated with the soft cells in panels (d3) and (d4) in Figure 4 of the main text.

396 **B.2. Soft 2D cells in fine art.** In the main text, Figure 3, we showed examples how some soft 2D cells appeared on facades of
 397 buildings designed by Zaha Hadid. Here we show two additional works of significant artists. Figure S24 shows a print by Victor
 398 Vasarely where we can not only observe soft 2D cells but also the metamorphosis of a rectangular grid into a soft tiling. Figure
 399 S25 shows three illustrations by Japanese artist Katsushika Hokusai, depicting patterns appearing in Japanese clothing as well
 400 as tatamis and rope curtains.

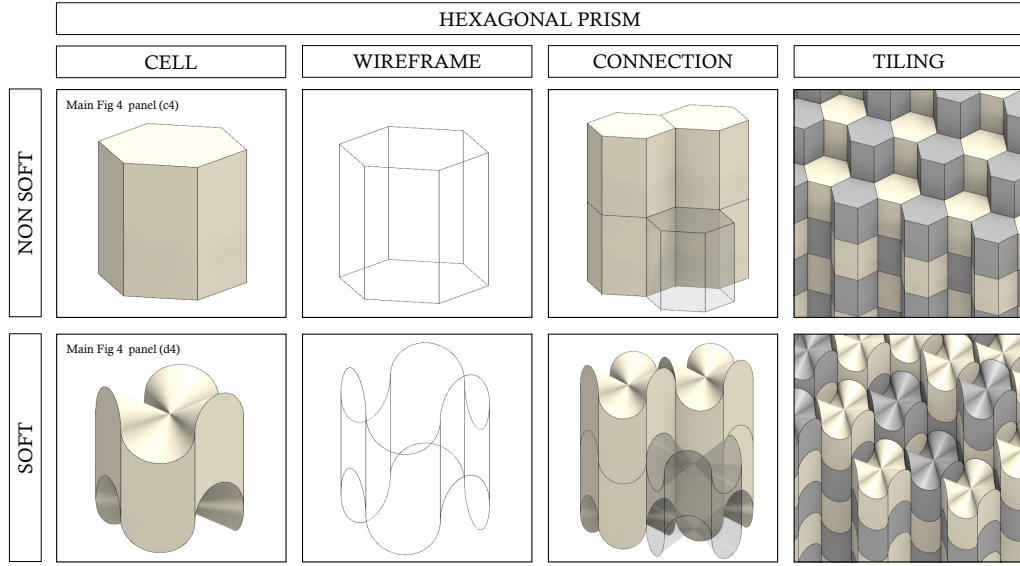


Fig. S19. The hexagonal prism cell. Detailed views of the soft cell shown in Figure 4, panel (d4) of the main text. Upper row: geometry of the space-filling non-soft cell from which the soft cell was constructed. Lower row: geometry of the soft cell.

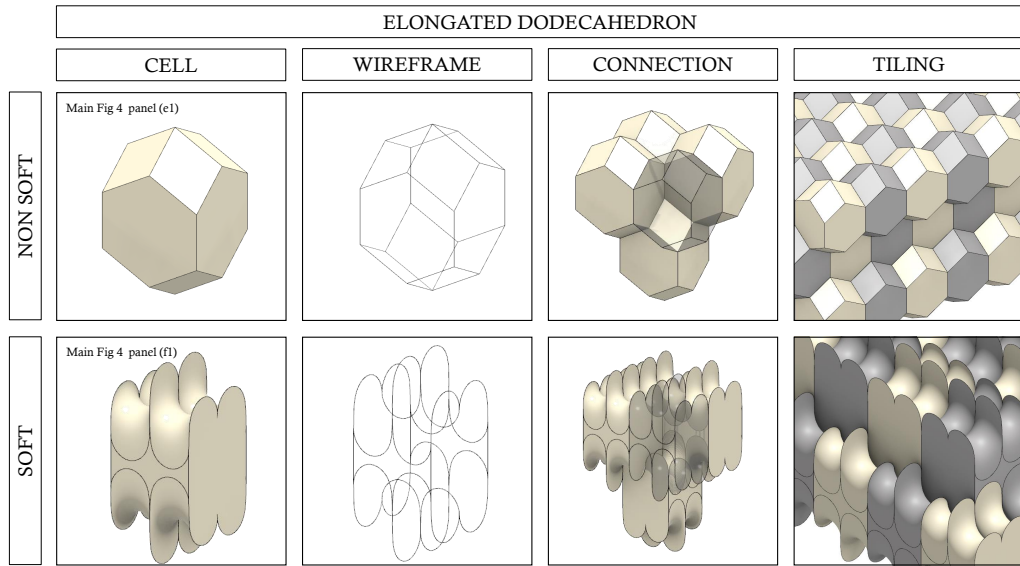


Fig. S20. The elongated dodecahedron cell. Detailed views of the soft cell shown in Figure 4, panel (f1) of the main text. Upper row: geometry of the space-filling non-soft cell from which the soft cell was constructed. Lower row: geometry of the soft cell.

401 5. Space filling properties of sea shell chambers

402 **A. Seilacher's models and the chamber of the Nautilus.** Any exact geometric claim on natural shapes (e.g. chambers of Nautilus
 403 and Ammonite shells) relies necessarily on some modeling step, performing intuitive simplification of these shapes. In our case
 404 this crucial step was taken by Adolf Seilacher who, in a series of seminal papers (9–11) formulated clear geometric models of
 405 these organisms, based on their growth process.

406 Seilacher described a broad range of models out of which here we discuss two, which, according to Seilacher, help to
 407 understand the geometry of the Nautilus chamber. Seilacher's *balloon model* approximates septa by an inflated balloon surface
 408 constrained into a circular or elliptical cylinder, with edges fully or partially glued to the inner surface of the cylinder. Seilacher's
 409 *paper model* approximates septa by intersecting a cylinder (of arbitrary basis) by a corrugated sheet and its copy under a finite
 410 translation along the axis of the cylinder.

411 Our definition of the z-cell (see main text, Materials and Methods, Definition 1) guarantees that, as long as the base of the

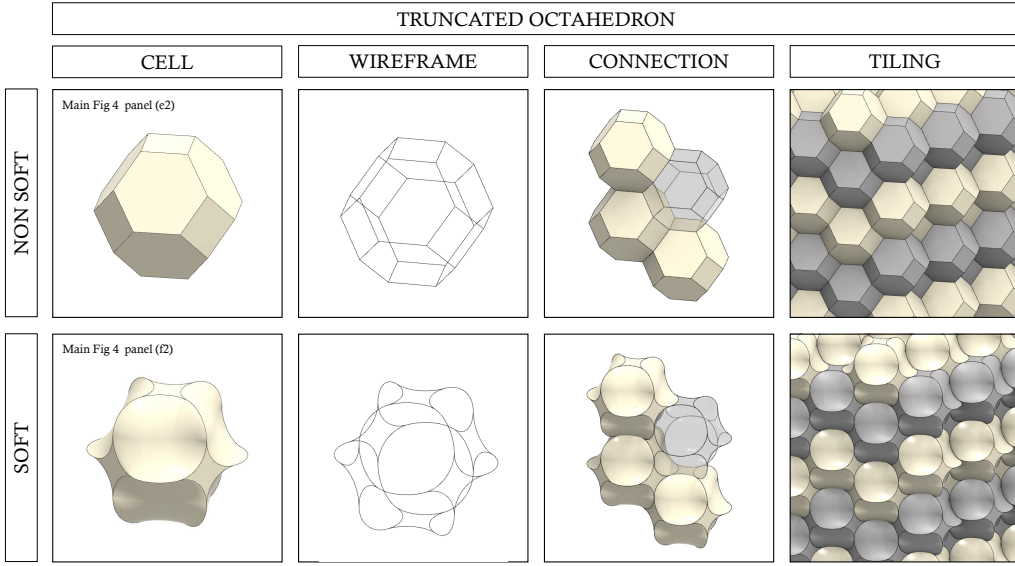


Fig. S21. The truncated octahedron cell. Detailed views of the soft cell shown in Figure 4, panel (f2) of the main text. Upper row: geometry of the space-filling non-soft cell from which the soft cell was constructed. Lower row: geometry of the soft cell.

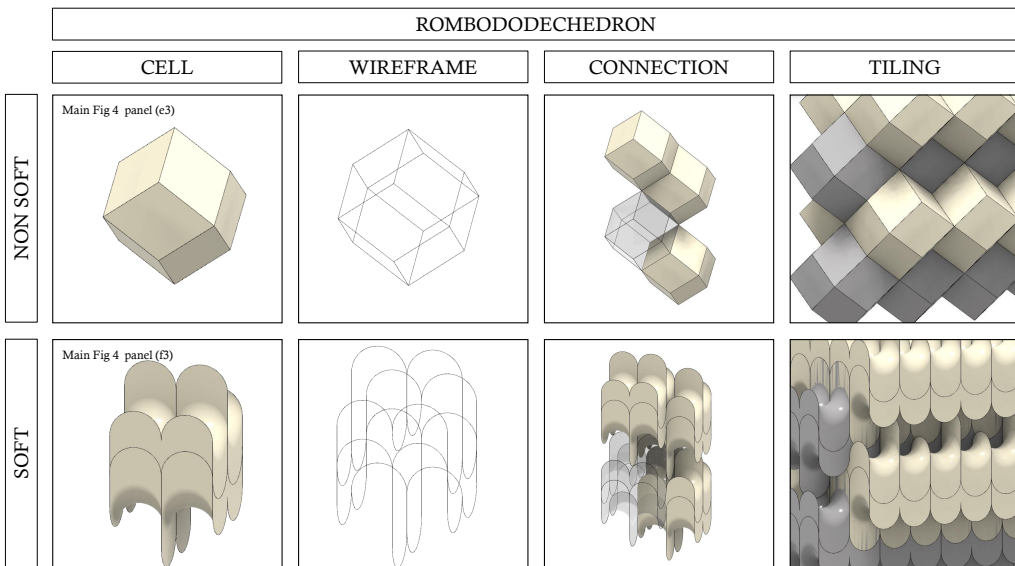


Fig. S22. The rombododecahedron cell. Detailed views of the soft cell shown in Figure 4, panel (f3) of the main text. Upper row: geometry of the space-filling non-soft cell from which the soft cell was constructed. Lower row: geometry of the soft cell.

412 cylinder is a smooth curve, Seilacher's balloon model always produces soft z -cells and that Seilacher's paper model generically
 413 produces soft z -cells.

414 Below we describe both models, relying on the terminology and notation of Definition 11 and explain that the balloon model
 415 explains important aspects of the Nautilus chamber's surface geometry while the paper model explains the geometry of its
 416 contour.

417 **A.1. The balloon model.** In the balloon model the flattened version of the lateral wall is approximated by a straight cylinder B ,
 418 with planar curve b_0 as base, and axis z . The septal wall is modeled by a surface of a balloon, placed inside B . Using the
 419 terminology of Definition 11, the balloon will be in contact with cylinder along the curve b_1 and the surface of the balloon will
 420 be denoted by \mathcal{M}_1 . We also consider its parallel z -translation \mathcal{M}_ϵ with contact line b_2 and these two surfaces define the finite
 421 segment \mathcal{B} of the infinite cylinder B . According to Seilacher (11), the finite surfaces $\mathcal{M}_\infty, \mathcal{M}_\epsilon$ are the geometric models of the
 422 *septal walls* (Septalfächen). In the balloon model, since the surface of the balloon is a smooth manifold, if b_0 is smooth then b_1

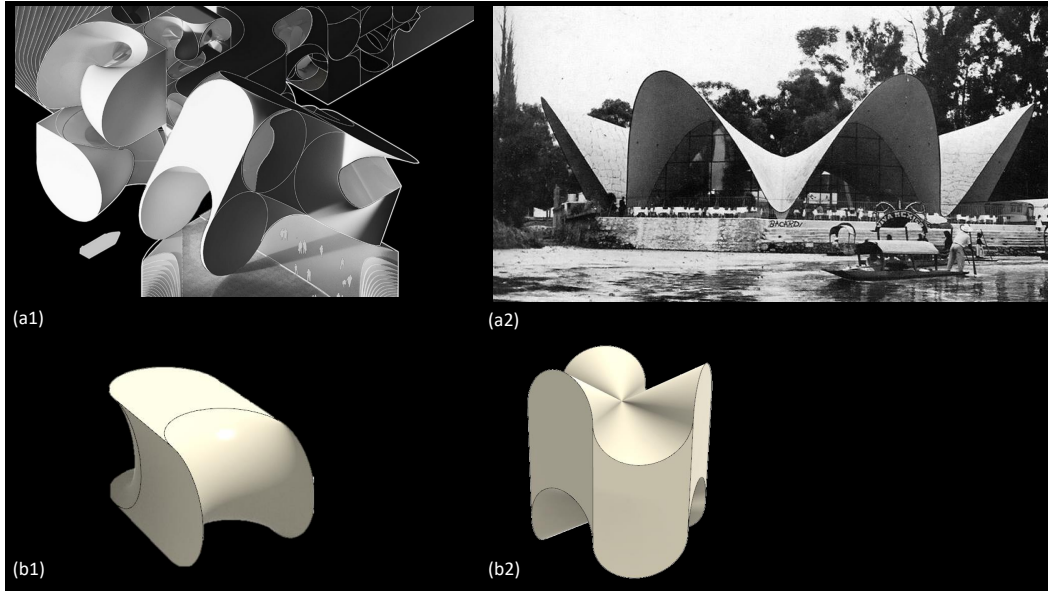


Fig. S23. Soft cells in architecture. (a1) Studio Hani Rashid (Lenka Petraková, Viki Sándor, Piotr K. Prokopowicz, Roman Hajtmánek): Conceptual design for the Cirque de Soleil Performance Centre, Brooklyn, New York. (2015). (b1) Soft, monohedric 3D cell from panel (d3) in Figure 4. of the main text. (a2) Felix Candela: Restaurant Los Manantiales, Mexico City, Mexico (1960). (b2) Soft, monohedric 3D cell from panel (d4) in Figure 4. of the main text.

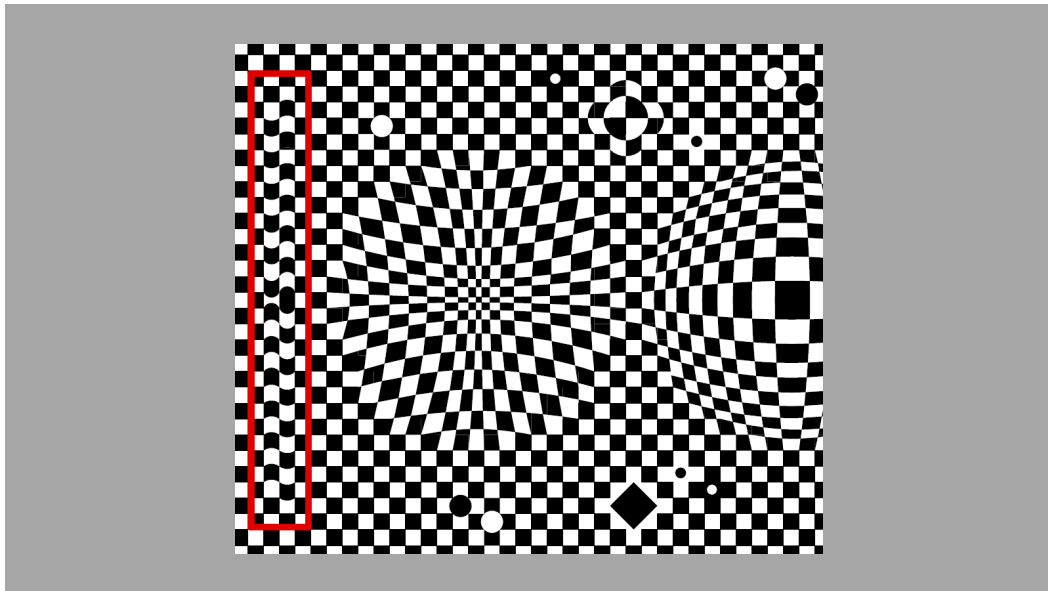


Fig. S24. Soft cells in fine art. Computer drawing illustrating some patterns appearing originally on *Vega* by Victor Vasarely (Date 1957/59. Technique: Screenprint on paper. Dimensions 505x600mm. Museum of Fine Arts, Budapest. Inventory number L68.118.) Red rectangle shows domain where soft cells emerge.

will also be smooth, and $i\mathcal{B}$ becomes a soft z -cell. In the simplest case discussed by Seilacher, the balloon is not attached to the cylinder by gluing, contact is established just by pressurizing the balloon. In this case, the tangent plane of the balloon and the tangent plane of the cylinder. When glue is applied at some parts of the cylinder, pulling the balloon downward leaves the contact line on the cylinder's boundary invariant at the glued locations, and the tangents of the balloon and the cylinder will intersect transversely. Since the contact curve b_1 remains smooth, \mathcal{B} will still remain a soft z -cell, despite the nonzero tangent angle. The left panels in Figure S26 show Seilacher's original drawings, as well as the geometric notations of Definition 11 and the curved surface in the Nautilus chamber approximated by the balloon's surface. Observe that, as predicted by the balloon model the Nautilus chamber's *surface* shows predominantly positive Gaussian curvature. Seilacher argued that, despite this qualitative agreement, the balloon model does not capture all essential features of the Nautilus chamber and to describe those, he also used the paper model which we discuss below.

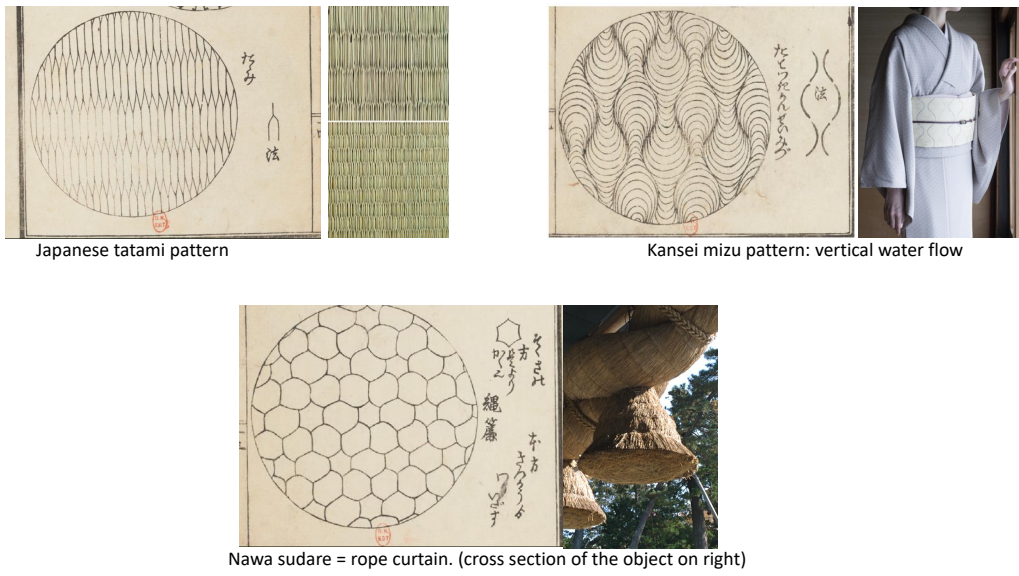


Fig. S25. Soft cells in fine art. Illustrations by Katsushika Hokusai: Album de petits motifs d'un nouveau modèle (1824) Source: gallica.bnf.fr / Bibliothèque nationale de France. Rope curtain photo: Yasuhiro Arakawa.

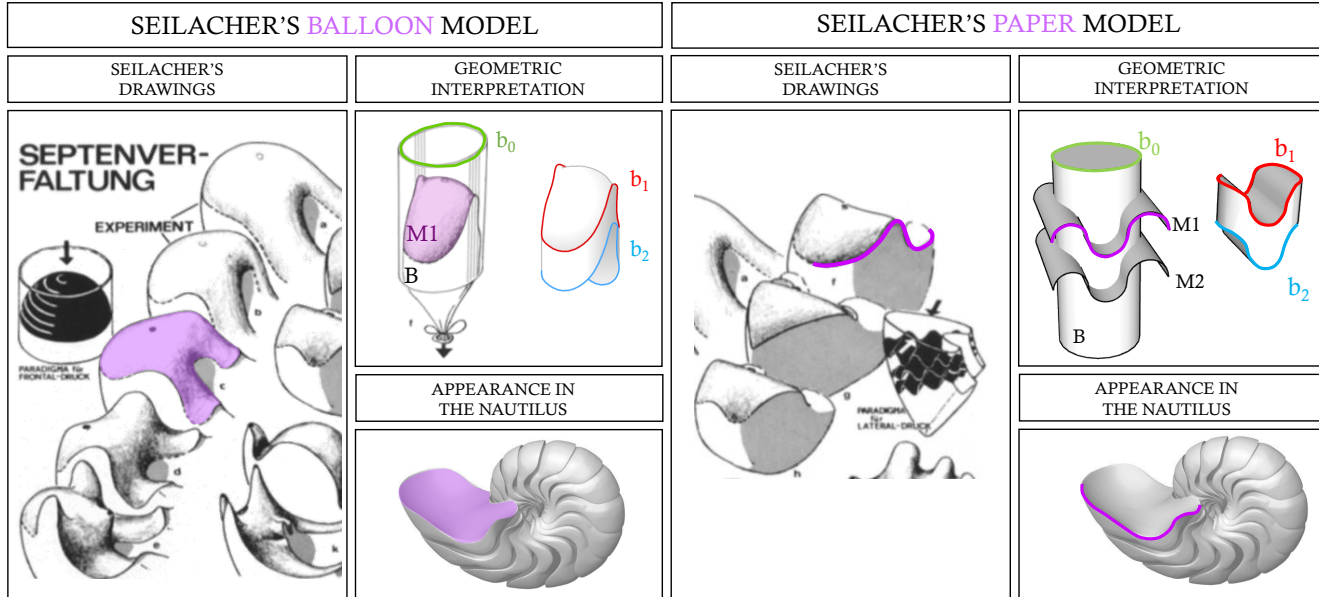


Fig. S26. The geometry of the Nautilus chamber reflected in Seilacher's models (11). Left panels: the balloon model. Model predicts positive Gaussian curvature (inflated balloon) and this is well reflected by the surface of the chamber. Right panels: the paper model. Model predicts sinusoidal contour and this is well reflected in the contour of the chamber.

433 **A.2. The paper model.** In the paper model we approximate (as before, in the balloon model) the flattened version of the lateral
 434 wall (Laterallobus) using the straight cylinder B with the planar curve b_0 as base and axis z . In the next step, B is intersected
 435 by a smooth, developable, corrugated surface M_1 with the property that at every point of M_1 we have a straight line contained
 436 in M_1 passing through that point and being orthogonal to the z axis. Cylinder B is also intersected by the parallel z -translation
 437 of M_1 which we will denote by M_2 . Here again, the respective intersections $\mathcal{M}_1, \mathcal{M}_2$ of the surfaces M_1, M_2 with the cylinder

438 B are the geometric models of the septal walls, the perimeter of which is traced by the space curves b_1, b_2 , respectively. This
439 defines a finite segment of B which we will denote by \mathcal{B} , and which is, according to Seilacher, the geometric model of the
440 shell chamber. Since M_1, M_2 are related by rigid body translation in the z direction, Definition 11 implies that \mathcal{B} is always a
441 primary z -cell. The right hand panels in Figure S26 illustrates Seilacher's original drawings, the geometrical concept with the
442 notations of Definition 11 and the Nautilus chamber with highlighted edge corresponding to the intersection with surface M_1 .
443 If b_0 is a 2-dimensional space-filling cell then, generically \mathcal{B} is a softened, spacefilling z -cell. Observe that, as predicted by
444 the paper model, the *contour* of the Nautilus chamber displays the sinusoidal pattern defined by the intersection manifold,
445 generating the z -cell.

446 **B. Ammonite shells.** Below we give the images illustrating the soft z -cell property of several ammonite shells as well as the
447 Nautilus shell. For the latter and for the Cadoceras shell we provided some images already in the main text, here we give a
448 more detailed view for each. All notations (in particular the notations for the contours b_0, b_1, b_2 are in accordance of Definition
449 1 in the Materials and Methods section of the main article.

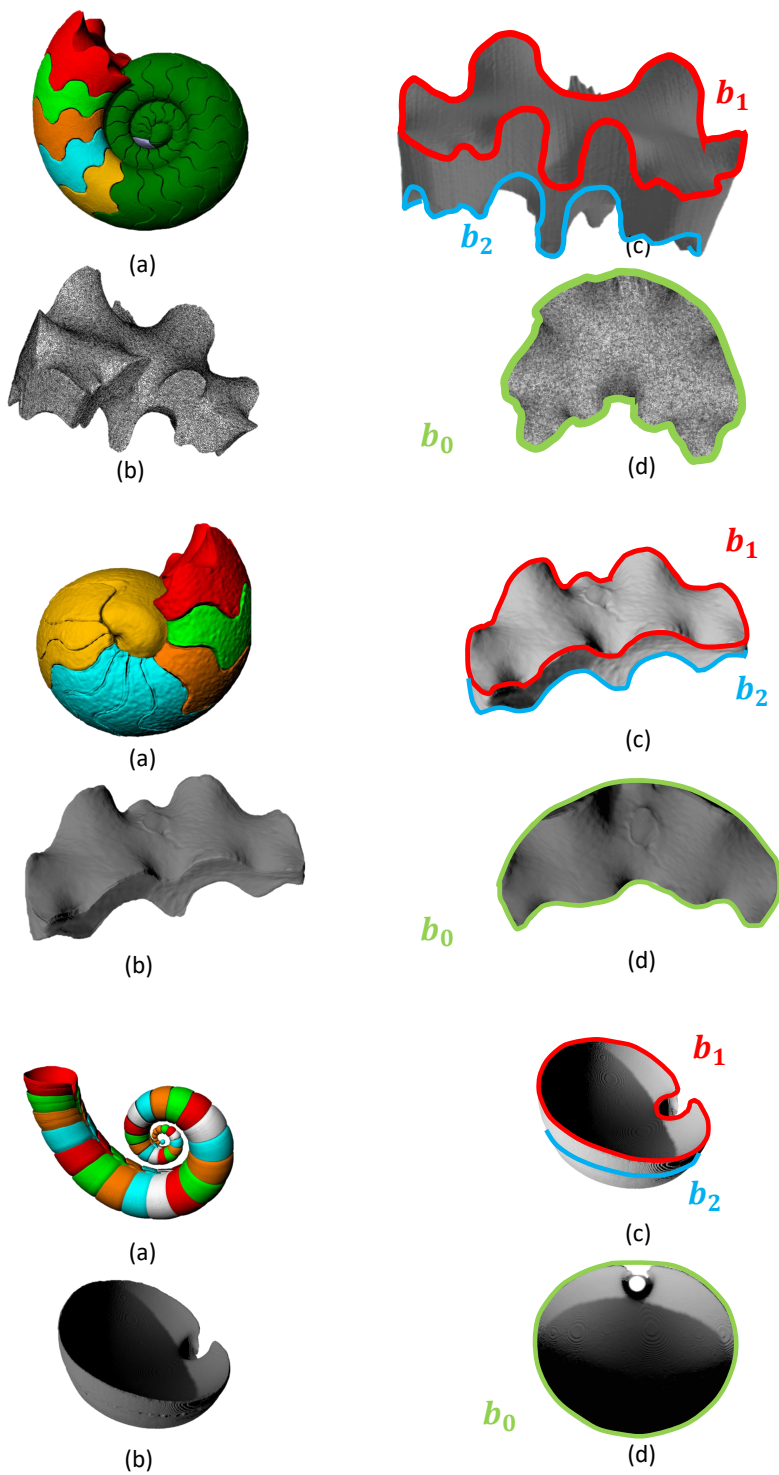


Fig. S27. Space filling property of the Amauroceras, Cadoceras and Spirula chambers. (a) All chambers, reconstructed from micro CT dataset (12). (b) Single chamber (c) Curves b_1 and b_2 traced on chamber. Observe that both curves are smooth. (d) Cross section curve b_0

- 450
451 1. B Grünbaum, G Shephard, *Tilings and Patterns*. (Freeman and Co., New York), (1987).
452 2. R Schneider, W Weil, *Stochastic and integral geometry*. (Springer Science & Business Media), (2008).
453 3. G Domokos, Z Lángi, On some average properties of convex mosaics. *Exp. Math.* (2019).
454 4. G Domokos, AG Horváth, K Regős, A two-vertex theorem for normal tilings. *Aequationes Math.* **97**, 185–193 (2023).
455 5. PG Tait, Listing's topologie. *Philos. Mag.* **5**, 30 – 46 (1884).
456 6. WT Tutte, On hamiltonian circuit. *J. Lond. Math. Soc.* **21**, 98 – 101 (1884).
457 7. M Goldberg, Three infinite family of tetrahedral space-filters. *J. Comb. Theory (A)* **16**, 346 – 357 (1974).
8. KMS Farin G., Hoschek J., *Handbook of Computer Aided Geometric Design*. (Elsevier), (2002).

- 458 9. A Seilacher, Mechanische simulation und funktionelle evolution des ammoniten-septums. *Paläontologische Zeitschrift* **49**, 268–286 (1975).
- 459 10. A Seilacher, Fabricational noise in adaptive morphology. *Syst. Zool.* **22**, 451–465 (1973).
- 460 11. A Seilacher, M Labarbera, Ammonites as cartesian divers. *PALAIOS* **10**, 493–506 (1995).
- 461 12. R Lemanis, D Korn, S Zachow, E Rybacki, R Hoffmann, The evolution and development of cephalopod chambers and their shape. *Plos One* (2016).